Improving solid freeform fabrication by laser-based additive manufacturing

D Hu, H Mei and **R Kovacevic***
Research Center for Advanced Manufacturing, Southern Methodist University, Richardson, Texas, USA

Abstract: Solid freeform fabrication (SFF) methods for metal part building, such as three-dimensional laser cladding, are generally less stable and less repeatable than other rapid prototyping methods. A large number of parameters govern the three-dimensional laser cladding process. These parameters are sensitive to the environmental variations, and they also influence each other. This paper introduces the research work in Research Center for Advanced Manufacturing (RCAM) to improve the performance of its developed three-dimensional laser cladding process: laser-based additive manufacturing (LBAM). Metal powder delivery real-time sensing is studied to achieve a further controllable powder delivery that is the key technology to build a composite material or alloy with a functionally gradient distribution. An opto-electronic sensor is designed to sense the powder delivery rate in real time. The experimental results show that the sensor's output voltage has a good linear relationship with the powder delivery rate. A closed-loop control system is also built for heat input control in the LBAM process, based on infrared image sensing. A camera with a high frame rate (up to 800 frame/s) is installed coaxially to the top of the laser–nozzle set-up. A full view of the infrared images of the molten pool can be acquired with a short nozzle–substrate distance in different scanning directions, eliminating the image noise from the metal powder. The closed-loop control results show a great improvement in the geometrical accuracy of the built feature.

Keywords: solid freeform fabrication (SFF), cladding, image sensing, control, powder delivery, sensor

NOTATION

A_f	measured area of the molten pool (pixel number)
A_r	preset reference area of the molten pool (pixel number)
C_1	first radiation constant $=1.191\,062 \times 10^8 \mathrm{W\,\mu m^4/m^2\,sr}$
C_2	second radiation constant $=1.438\,786 \times 10^4\,\mu\mathrm{m\,K}$
e	error $= A_r - A_f$ (pixel number)
E_λ, E	spectral radiance ($\mathrm{W/m^2\,sr}$)
K_d	proportional control gain (dimensionless)
K_f	feedforward control gain (dimensionless)
K_i	integral control gain ($\mathrm{s^{-1}}$)
k_p	derivative control gain (s)
P	laser mean power percentage (per cent)
T	temperature (K)
T_{mes}	measured spectral radiance temperature of the target (K)
T_{true}	true temperature of the measured target (K)
W_a	averaged width (mm)
W_{min}	minimum width (mm)
ε_λ	spectral emissivity
η	geometrical variation coefficient (per cent)
λ	wavelength (μm)

The MS was received on 27 December 2001 and was accepted after revision for publication on 13 May 2002.
**Corresponding author: Research Center for Advanced Manufacturing, Southern Methodist University, 1500 International Parkway, Suite 100, Richardson, TX 75081, USA.*

1 INTRODUCTION

Building metal parts with a good accuracy and mechanical properties for functional prototypes and products is one of the primary aims of solid freeform fabrication (SFF). Several SFF methods have been developed to produce metal parts, such as three-dimensional welding [**1**, **2**], micro casting [**3**], selective laser sintering (SLS) [**4**], laser-engineered net shaping (LENS) [**5**], shape deposit manufacturing (SDM) [**6**], directed-light fabrication (DLF) [**7**], three-dimensional cladding [**8**, **9**] and some hybrid methods [**10**, **11**]. Compared with other SFF methods, three-dimensional laser cladding has several advantages. In general, laser processing can produce relatively more accurate results. Because of the

powder delivery feature in three-dimensional laser cladding, no inert-gas protection chamber is required. So a larger part can be produced, and a more complicated cladding path can be traced including four-dimensional and five-dimensional paths. By controlling the mass delivery rate of the metal powders from the different powder feeders, a composite material or alloy with a functionally gradient distribution can also be produced.

The SFF methods for metal part building suffer more instability and irrepeatability problems than other rapid prototyping methods. In three-dimensional laser cladding, a large number of parameters govern the cladding process [**12**]; they are sensitive to the environment variations and influence each other. A first set of parameters is related to the equipment used: the laser, the focusing and the beam-shaping optics, the nozzle, the powder and gas delivery system, and the substrate on a moving stage. Another group of parameters is related to the interaction zone. There are two interaction zones. One zone is the space below the nozzle exit and above the substrate where the powder interacts with the laser. The second zone is located at the substrate surface where a molten pool is formed by the heat of the laser, and the powder is projected into the molten pool to adhere to the substrate. Several research studies have reported improvements in the laser cladding process. Some of the research focuses on controlling the powder delivery system in order to achieve a stable or controllable powder delivery [**13**, **14**], or to study the powder stream distribution and laser–powder interaction [**12**, **15**]. Other investigations deal with the optimization of the laser cladding process with closed-loop control, using a charge-coupled device (CCD) camera [**16**–**19**] or phototransistor [**20**] as the sensing device.

The controllable powder delivery can greatly improve the performance of three-dimensional laser cladding. It provides the feasibility to build a functionally gradient material or alloy. The key component for achieving powder delivery control is a real-time powder delivery rate sensing unit. Most commercial powder delivery systems use continuous weight measuring for a feedback. The weight-measuring method has a large time delay to achieve the desired stable powder delivery rate. Some research work provides different methods for real-time powder delivery rate sensing, such as applying an opto-electronic sensor [**13**], and increasing the weight sampling rate by modifying the structure of the powder feeder [**14**], but those studies are specific to the particular powder feeders and focus on the applications of two-dimensional surface cladding.

The sensing of the molten pool to control three-dimensional laser cladding is of great importance. A few attempts on sensing the molten pool have been reported which utilize infrared imaging as a sensing method acquired by a CCD camera [**16**–**19**] or a phototransistor [**20**]. However, the CCD camera or the phototransistor is usually installed from one side of the nozzle. This installation is not practical for SFF three-dimensional cladding. The distance between the nozzle and the substrate is very small (about 5 mm); therefore, the field of view is heavily limited. The images are deformed due to the angle between the optical central line of the camera and laser–nozzle set-up. Also, the images acquired from an asymmetrically installed camera vary because of the lack of omnidirectionality. A coaxial installation of the camera has great advantages for molten pool sensing [**19**].

In this paper, the research efforts in Research Center for Advanced Manufacturing (RCAM) to develop its three-dimensional laser cladding, i.e. laser-based additive manufacturing (LBAM), are introduced. Sensing and control technologies are applied to improve the overall performance of the LBAM process for SFF. Real-time sensing of the metal powder delivery rate is studied. An opto-electronic sensor is designed to sense the powder delivery rate in real time. The experimental results show that the sensor's output voltage has a linear relationship with the powder delivery rate. A closed-loop control system is also developed for heat input control in the three-dimensional laser cladding process, based on infrared image sensing. A CCD camera with a high frame rate (up to 800 frame/s) is installed coaxially to the top of the laser–nozzle set-up. A full-view infrared image of the molten pool and surrounding area can be easily acquired with a short nozzle–substrate distance and different scanning directions, eliminating the noise from the metal powder. The experimental results of closed-loop control show great improvement in the geometrical accuracy of the part being built.

2 REAL-TIME SENSING OF METAL POWDER DELIVERY

The controllable powder delivery can greatly improve the performance of three-dimensional laser cladding. It provides the feasibility to build a functionally gradient material or alloy. The key technology for implementing powder delivery control is real-time sensing of the metal powder delivery. The LBAM is equipped with a commercial powder delivery system designed for a plasma-spraying process in which a higher powder delivery rate is desired. The powder feeder is equipped with an electronic weight scale to measure continuously the weight of the metal powder inside the hopper, and it uses the change in weight as a feedback to control the powder delivery rate. Because of the low sampling frequency of the feedback, a steady delivery rate can only be realized if the delivery rate is averaged over a long period of time after the feed screw reaches a stable rotational speed. On a smaller time scale, fluctuations in powder delivery can be observed.

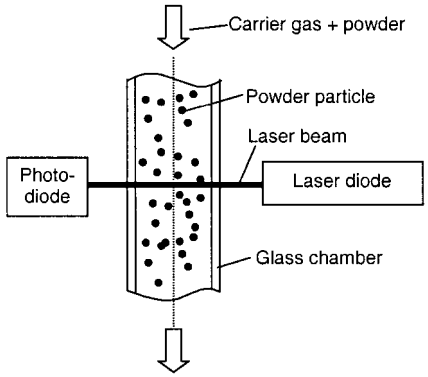

(a) Schematic of the powder delivery rate sensor

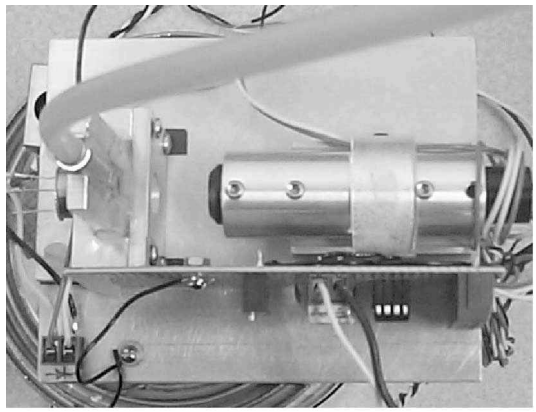

(b) Setup of the powder delivery rate sensor

Fig. 1 Powder delivery rate sensor

An opto-electronic sensor is developed to sense the metal powder delivery rate in real time. The sensor consists of a laser diode, a photodiode and a glass window. The components are installed in such a way that the laser beam emitted from the laser diode passes through the powder stream flowing inside the glass chamber and is received by the photodiode (Fig. 1a). The carrier gas and the metal powder are mixed well so that the powder particles are distributed uniformly in the carrier gas. Because of the diffusion, absorption and reflection of the powder particles in the laser beam, the laser energy received by the photodiode is decreased if the powder delivery rate is increased, which means that there is a higher percentage of powder particles in the carrier gas. The laser diode emits a red light with a wavelength of 600–710 nm and with a power less than 500 mW. The photodiode is characterized with a good linearity between the illumination energy received by the diode and the output current that is converted later to a voltage signal through a current signal pick-up circuit. Figure 1b shows the set-up of the metal powder delivery rate sensor.

A group of experiments is set up to test and calibrate the sensor. By setting the feed screw of the powder feeder at different rotational speeds, a series of powder

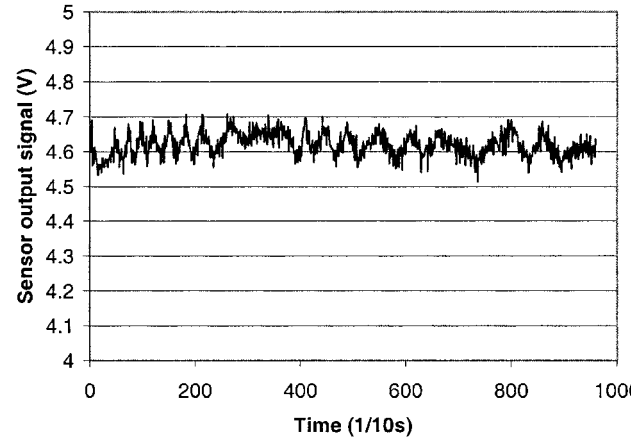

Fig. 2 Sensing signal for a screw rotational speed of 50 r/min

delivery rates can be obtained. The feed screw runs at the preset rotational speed for about 2 min before any measurement is taken to ensure that a static delivery status has been reached. The averaged powder delivery rate is then calibrated by measuring the time period and the weight of the powder delivered during that time period. The corresponding sensing signal from the sensor is also acquired at 10 Hz by a data acquisition card installed on a personal computer (PC). As can be seen from the sensing signal for a certain screw rotational speed given in Fig. 2, the signal has a stable averaged value that represents a steady averaged powder delivery rate under that screw rotational speed; meanwhile, the higher-frequency signal variation reflects the fluctuation in the powder delivery. The averaged sensor output voltage presented in Fig. 3 exhibits a nearly linear relationship to the averaged powder delivery rate in the range 3–22 g/min. In the LBAM process, the powder feed rate is below 15 g/min. In this range, the sensor provides a good sensing and feedback feature for the further control of the metal powder delivery rate.

The sensing signal of the powder delivery rate from the developed sensor is utilized as feedback to control the rotational speed of the feed screw. The real-time sensing at a higher sampling frequency provides the powder feeder with the feasibility of more even and controllable powder delivery. Precise delivery of the functionally gradient material can also be implemented on the basis of powder delivery sensing and simultaneously controlling multi-powder feeders. The metal powder delivery rate control and functionally gradient material delivery based on the developed sensor will be studied in further research work.

3 DEVELOPMENT OF INFRARED IMAGE ACQUISITION SYSTEM

Infrared imaging of the molten pool is a promising sensing method for controlling the LBAM process for

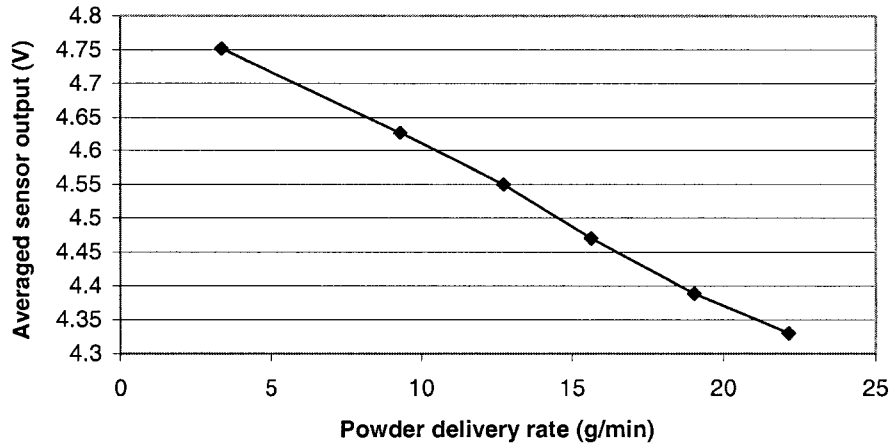

Fig. 3 Output performance of the powder delivery rate sensor

the following reasons:

1. It directly monitors the last and most important stage of the build-up process, in which the powder is melted inside the molten pool and forms the bead. The changes in the process parameters eventually influence the shape and the temperature of the molten pool.
2. The infrared images of the molten pool reflect the temperature information that strongly affects the cladding results. The temperature of the molten pool is sensitive to variations in the processing parameters, such as the scan path and velocity, the laser absorption rate of the substrate surface, the cooling conductions and the rate of powder delivery. The laser absorption rate of the surface can be changed according to the surface qualities such as roughness, colour and temperature. The cooling conductions of the cladding area may change dramatically due to the complex geometrical shape of the part. The scan path arrangement also affects the cooling conditions by reheating.
3. The infrared image eliminates the image noise caused by the metal powder and is easy to process in real time. Without the infrared filter, the quality of the acquired image is degraded due to the existence of the metal powder particles in the image. No satisfactory image-processing result can be obtained because of the noise from the metal powder particles. When an infrared filter is applied, only areas with a high radiation energy can be acquired by the camera. Although the metal powder particles are heated in the laser–powder interaction zone, the particles never reach the melt temperature before they arrive in the molten pool. Radiation from the powder particles is totally covered by radiation from the molten pool which has a much higher temperature and greater mass. No powder particle outside the molten pool can be observed in the infrared image.

The main difficulty of infrared image sensing in LBAM arises from the short distance between the nozzle and the substrate (about 5 mm). This distance blocks the sight if the observation is from the sides of the nozzle. In order to observe the molten pool of cladding from one side, the camera is usually installed at a large angle with the central line of the nozzle set-up. The image acquired is distorted due to that angle as well as due to the direction of the motion. This problem will be exaggerated when the scanning path is multi-dimensional where the part could come into conflict with the camera or with the direction of observation.

A coaxially installed infrared image sensing set-up with respect to the metal powder delivery nozzle is introduced in this section to solve this problem. As shown in Fig. 4, the laser head consists of a partial reflective mirror and lens set. The neodymium-doped yttrium aluminium garnet (Nd: YAG) laser beam induced by the optical

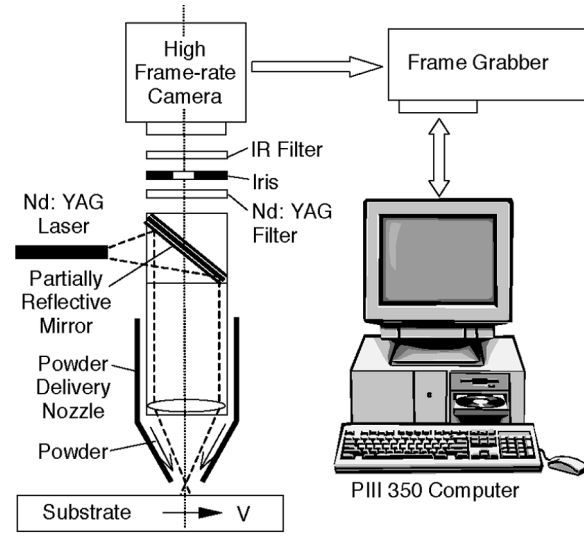

Fig. 4 Infrared image acquisition system

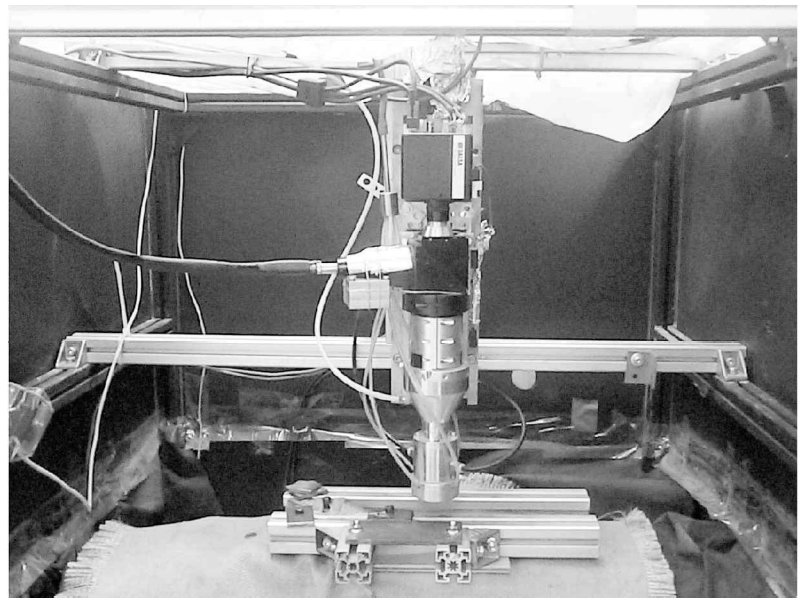

Fig. 5 Set-up of infrared image acquisition system

fibre is reflected from the partial reflective mirror, and it is focused on the substrate by the set of lenses arranged in the laser head. The optical part of the laser head forms another optical path for observation of the laser processing. A high frame-rate (up to 800 frames/s) camera is installed on the top of the laser head, taking grey images with a 128×128 resolution. The radiation from the molten pool produced by the laser beam passes through the partial reflective mirror and forms an image on the CCD chip of the camera. A Nd: YAG laser blocker (1.06 μm) is utilized to protect the camera from laser damage. An iris is used to adjust the intensity of the radiation received by the camera to prevent overexposure. In order to obtain the infrared image of the molten pool that reduces the high-intensity light from the molten pool and eliminates the image noise from the metal powder, an infrared filter is selected (greater than 700 nm) and installed between the iris and camera. During the LBAM process, the camera acquires images of the build-up process at a constant frame rate. Images are transferred to a frame grabber installed on a PC that carries out the image-processing and control process. The real set-up of the infrared image acquisition system is shown in Fig. 5.

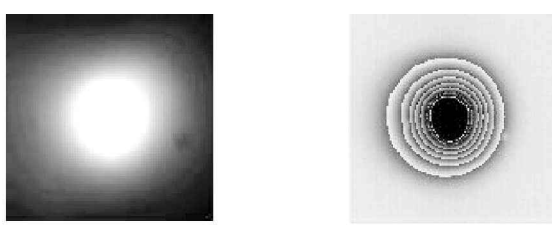

(a) Original infrared image (b) Grey level isotherms

Fig. 6 Infrared image acquired

Figure 6a provides the original infrared image acquired by the coaxially installed camera. Because the observation is directly from the top of the molten pool, a full field of view of the molten pool can be acquired without any blocking. With the correct combination of the Nd: YAG filter and the infrared filter as well as correct adjustment of the iris, a clear image of the molten pool and the surrounding thermal area can be obtained without the noise from the metal powder. The radiation wavelength received by the camera is between 0.7 and 1.06 μm.

The infrared images acquired reflect the temperature distribution around the molten pool. In 1901, Max Planck established the relationship between the intensity of electromagnetic radiation and its wavelength for any surface temperature. Planck's equation describes a continuum of the radiation wavelength. According to Planck's law, the spherical or total radiance is linked to the temperature of a black body by the following equation:

$$E(T, \lambda) = \frac{C_1}{\pi \lambda^5} \exp\left(\frac{-C_2}{\lambda T}\right) \tag{1}$$

where C_1 and C_2 are Planck's constants. Using Planck's law, the true temperature from the measured temperature can be inferred through the relation

$$E_\lambda(T_{\text{mes}}) = \varepsilon_\lambda E_\lambda(T_{\text{true}}) \tag{2}$$

The temperature measurement equation for the spectral room temperature using Wien's law (approximation of Planck's law for $C_2 \gg \lambda T$) for black-body spectral radiance takes the familiar form

$$\frac{1}{T_{\text{true}}} = \frac{1}{T_{\text{mes}}} + \frac{\lambda}{C_2} \ln \varepsilon_\lambda \tag{3}$$

where ε_λ is the target emissivity.

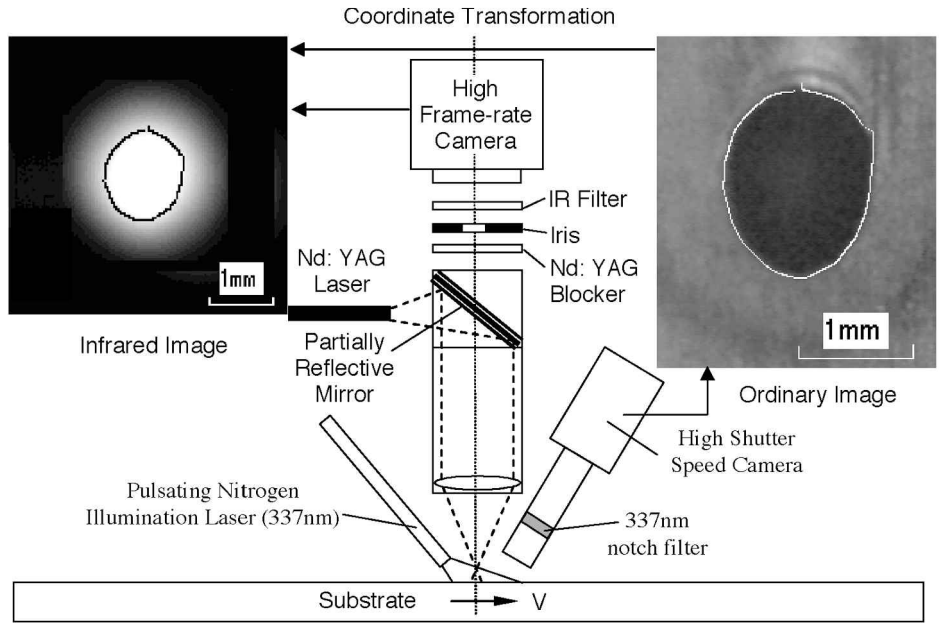

Fig. 7 Molten pool edge determination for infrared image

Meriaudeau *et al.* [**16**] calibrated the CCD camera with an infrared filter using a black body and concluded that the grey level of the pixel has a linear relationship with the temperature of the black body. For a real-target temperature measurement, the emissivity of the target is different from the black body due to the surface quality and temperature. The effect of the uncertainty in the spectral emissivity can be found by differentiating the temperature T_{true} with respect to ε_λ holding T_{mes} constant, as shown by

$$\frac{\Delta T_{\text{true}}}{T_{\text{true}}} = \frac{\lambda T_{\text{true}}}{C_2} \frac{\Delta \varepsilon_\lambda}{\varepsilon_\lambda} \tag{4}$$

which indicates that the linear relationship between the pixel grey level and temperature is still kept.

Figure 6b shows the grey level isotherms of the infrared image that indicate the temperature distribution in the molten pool and surrounding area. In order to determine the grey level value corresponding to the liquid–solid transient edge of the molten pool in the infrared image, an ultra-high shutter speed camera with a pulsed nitrogen laser is installed on the side of the laser head. The powder delivery nozzle is removed to provide a sufficient installation space and to ensure an undisturbed view under the Nd: YAG laser head for the high-shutter-speed camera. Calibrations for the physical dimensions of both cameras are accomplished first by taking images of a referenced target. Then, the ordinary and infrared images of the molten pool are acquired simultaneously by synchronizing the two cameras while the Nd: YAG laser is projected on the moving substrate. The pulsating nitrogen laser emits light with a wavelength of 337 nm to provide an illumination in the laser-processing area for the high-shutter-speed camera. A notch filter of 337 nm is also installed inside the high-shutter-speed camera, which allows light with a wavelength of only around 337 nm to pass. The pulsating illumination synchronized with the high-speed shutter on the camera suppresses the intensive light from the molten pool and ensures the successful acquisition of clear images of the molten pool. The ordinary images acquired from the high-shutter-speed camera are processed with a Canny edge detector to find the edge of the molten pool [**18**]. By mapping the position of the edge of the molten pool from the ordinary image to the corresponding infrared image through a coordinate transformation, it is determined that a grey level of 70 represents with enough accuracy the transition between the molten pool and the surrounding solid (Fig. 7).

4 CLOSED-LOOP CONTROL SYSTEM FOR HEAT INPUT CONTROL BASED ON INFRARED SENSING

The LBAM system consists of four subsystems: a 1 kW Nd:YAG laser source, a metal powder delivery system, a three-axis positioning system and an infrared image acquisition system. The three-dimensional metal part is produced layer by layer by synchronizing the X–Y–Z motion, the Nd:YAG laser and the injection of metal powder. The infrared image acquisition system takes the images of the molten pool in real time and calculates the dimensions of its area. It compares the recorded information with the preset value and creates a feedback control value to modify the output of laser source. In this way, a stable molten pool or its corresponding thermal field area with desired dimensions is obtained, and thus

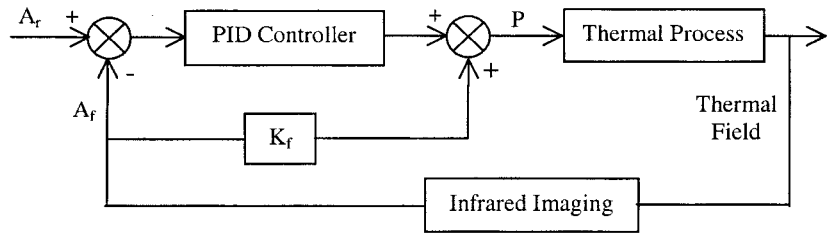

Fig. 8 Schematic diagram of the closed-loop control system

it is possible to produce stable and repetitive layers if a stable powder flowrate is ensured.

A simple proportional–integral–derivative controller is applied to build the closed-loop control system. Because of the existence of some 'lag' (less than 100 ms) in laser-computer parallel port communication, feedforward compensation is also introduced for control of the molten pool area. The schematic diagram of the control system is shown in Fig. 8. The control algorithm can be expressed as

$$P = K_p e + \frac{1}{K_i}\int e\,dt + K_d\frac{de}{dt} + K_f A_f \tag{5}$$

In the equation above, K_p is the proportional control gain (dimensionless), K_i is the integral control gain ($1\,s^{-1}$), K_d is the derivative control gain (s), e is the error defined by $e = A_r - A_f$, where A_r is the reference area of the molten pool and A_f is the measured area of the molten pool, K_f is the feedforward control gain and P is the laser mean power percentage command sent to the Nd: YAG laser controller to control the laser power. The relationship between the laser output power and mean power percentage is calibrated. The output value of P is between 40 and 100.

Two single-bead walls are built respectively by an open-loop and closed-loop controlled LBAM process to compare the processing results. The scanning path planning for building the single-bead wall is shown in Fig. 9 with the arrows indicating the direction of motion. The nozzle moves along the positive direction of the X axis first to build one layer, moves up for a small increment along the Z axis after the layer is built up and then moves back along the negative direction of the X axis for the next layer's deposition. The solid line indicates the path segments in which the laser shutter is open, and the laser cladding is processed on the previous layer. When the nozzle moves into the dashed-line path segments, the laser shutter is closed and no laser energy is projected. The threshold for counting the area of the molten pool in the number of pixels is set to 70, indicating the grey level of the edge of the molten pool. The images are recorded continuously with an image-processing rate of 15 frames/s during the wall building. The substrate material utilized in the experiments is mild steel, and the metal powder is an H13 tool steel powder with a +100/−325 mesh size. The powder delivery rate is kept constant.

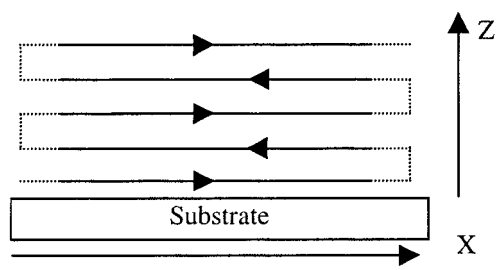

Fig. 9 Scanning path for single-bead wall building

A 50-layer single-bead wall is built first by the uncontrolled LBAM process. The processing parameters utilized in the experiment are a 5 mm/s scanning speed, a 4 g/min powder delivery rate, a 0.25 mm Z-height increment and a 420 W constant laser power. Figure 10 shows the signal of the molten pool area for numbers of pixels greater than the preset threshold. The number of frames can be regarded as the processing time due to the constant image acquisition rate. Each pulse in Fig. 10 represents one cladded layer. Figure 10a displays the signal of the whole process, from which the overall variation trend can be observed. The zoomed-in signal for two selected layers is given in Fig. 10b. This signal provides information on the variation in the molten pool area along one cladded layer. The finished part is shown in Fig. 11.

The uncontrolled LBAM is affected by the changes in the heat loss. At the beginning of the wall building, due to the large heat conduction of the substrate, the created beads are narrower. As the wall grows, there is less heat conduction along the built wall, and the bead becomes wider until it reaches a new equilibrium value. From the cross-section of the wall shown in Fig. 11b, it can be seen that the base of the wall is narrower than the upper layers. It can also be observed from Fig. 10a that the pixel number of the molten pool area is 4000 for the first layer and gradually increases to around 10 000. The molten pool area also changes along one cladded bead. The two ends of the bead have less time to cool than the middle segment of it. Therefore, without laser power control, the two ends of the bead can reach a higher temperature reflected by the peak of molten pool area shown in Fig. 10b. The higher temperature

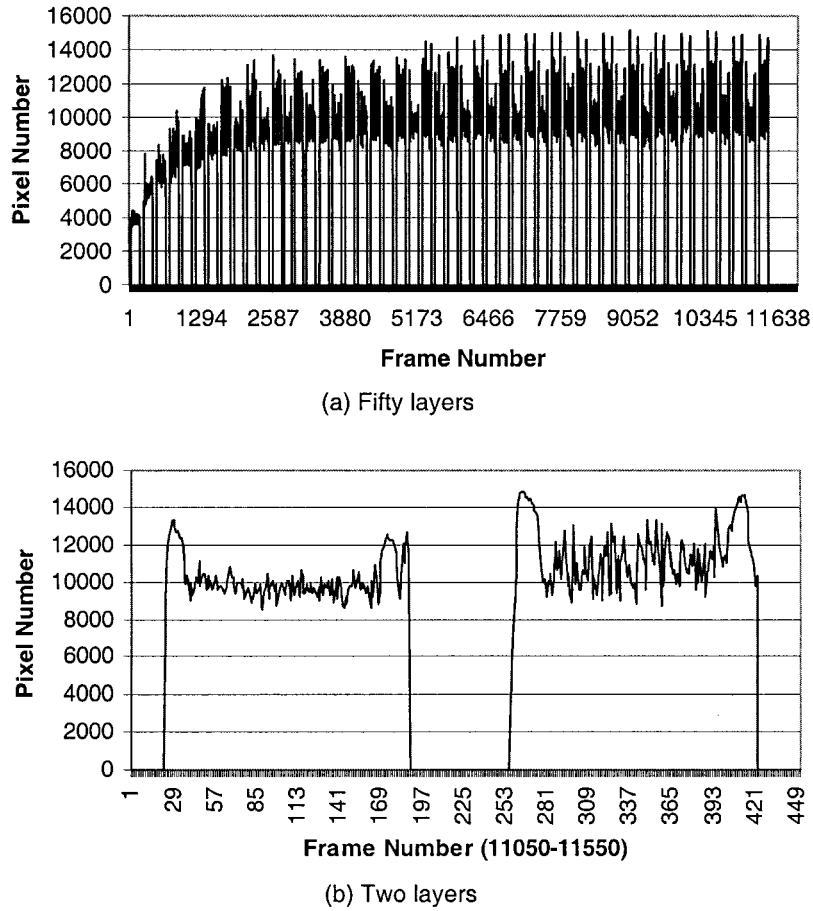

Fig. 10 The area of molten pool in three-dimensional laser cladding

results in more powder melting and cladding and causes the higher build-up at both ends of the wall that can be seen in Fig. 11a. It is a very common situation in three-dimensional laser cladding that heat loss varies according to the part's geometric features and scanning paths. Thus, without a closed-loop control, LBAM cannot provide uniform geometry of the built layers.

Closed-loop controlled LBAM is carried out using the same processing parameters to build a 60-layer single-bead wall in order to test the performance of the developed control system. The reference value of the molten pool area is set to 5000. The molten pool area and laser power control signals are presented in Fig. 12. Figure 13 shows the built part.

The closed-loop controlled LBAM system shows a very good performance. As shown in Fig. 12a, the molten pool area is controlled around the reference value during the wall building process. The laser power is decreased from 80 per cent to about 60 per cent to keep the molten pool constant (Fig. 12b). In one

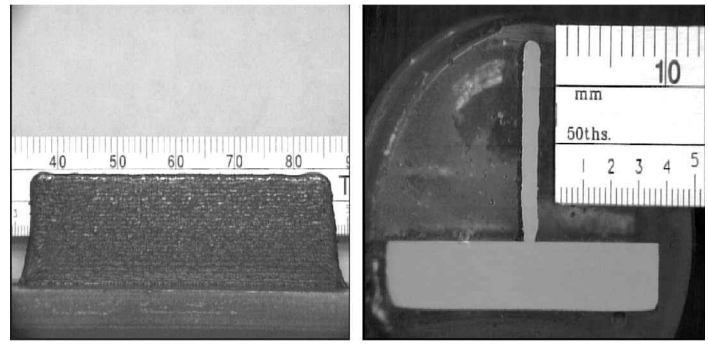

Fig. 11 Single-bead wall built by an uncontrolled three-dimensional laser cladding process

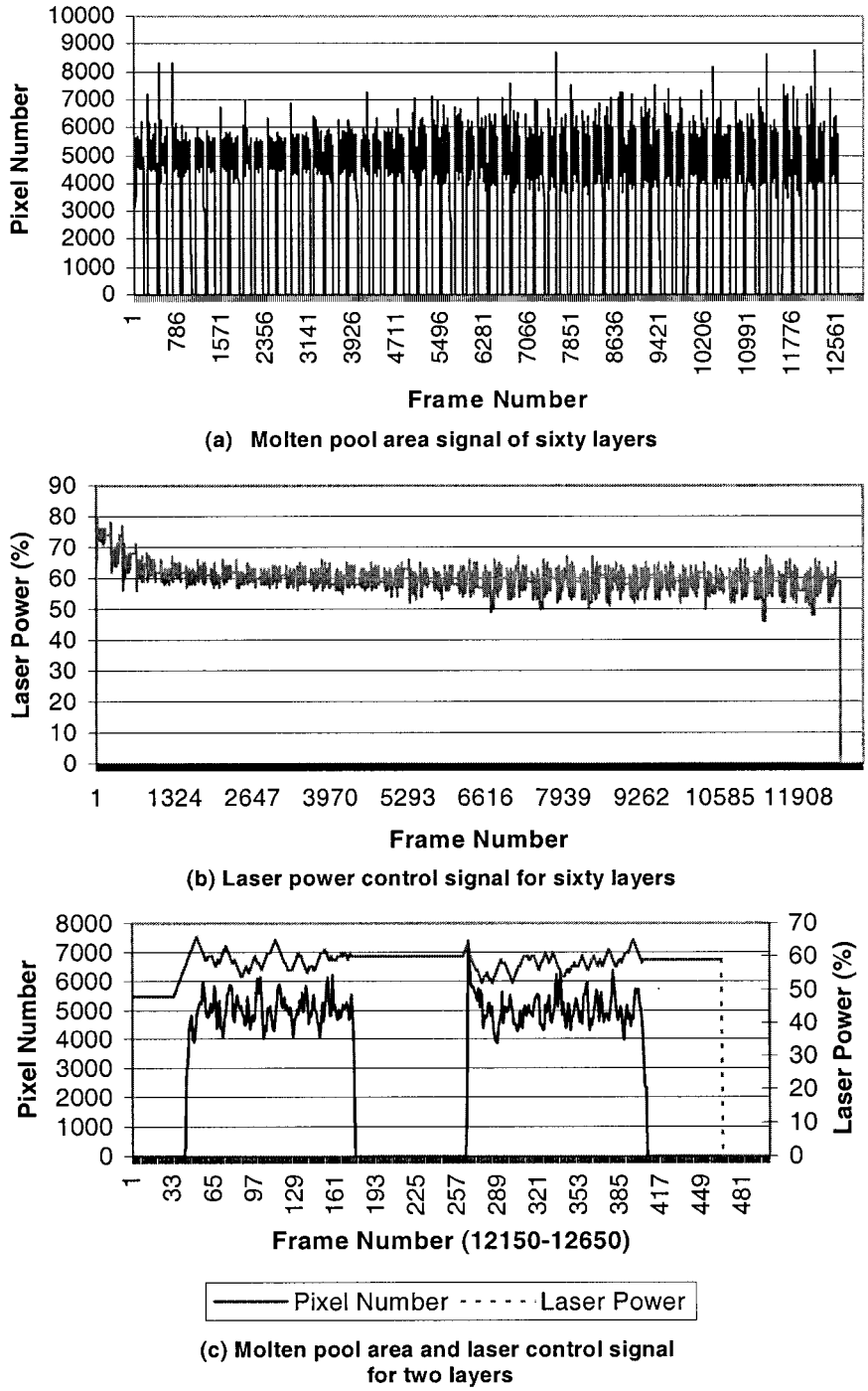

Fig. 12 Molten pool area and laser control signals in closed-loop three-dimensional laser cladding

single-bead cladding process, the increase in the molten pool area at the both ends of the bead indicating the higher temperature is reduced due to the action of the closed-loop control. The built wall shown in Fig. 13 is characterized by a uniform geometry. There are no build-ups at the end of the wall. From the cross-section of the wall, it can be seen that the width of the wall is constant.

To compare the processing results further, single-bead walls are built under the following three processing conditions [**9**]. The first type of sample is built with no preheating to the substrate and no closed-loop control of the heat input. The second type of sample is built with preheating but no control, and the third type of wall is built utilizing the closed-loop control function without preheating.

The geometrical parameters of cross-sections of the walls built in different processing conditions are given in Table 1. The average width of the wall W_a is calculated by averaging ten width measurements taken at ten evenly

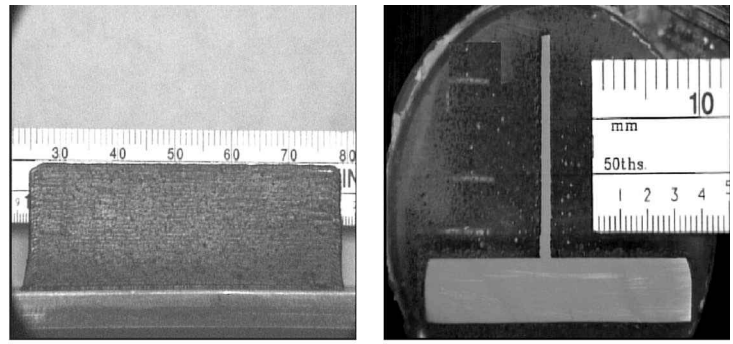

Fig. 13 Single-bead wall built by a closed-loop-controlled three-dimensional laser cladding process

Table 1 Geometry of the walls built under different conditions

	Without preheating and without control			With preheating and without control			With control and without preheating*		
Laser power (W)	W_a (mm)	W_{min} (mm)	η (%)	W_a (mm)	W_{min} (mm)	η (%)	W_a (mm)	W_{min} (mm)	η (%)
290	0.95	0.45†	53	0.95	0.62	35	0.91	0.90	1
370	1.33	0.58	56	1.26	0.90	29	1.02	1.01	1
450	1.48	0.79	47	1.50	0.94	37	1.35	1.15	15
540	1.61	0.95	41	1.60	1.00	38	1.58	1.29	19
620	1.70	0.99	42	1.75	1.00	43	1.67	1.31	22

* The laser powers listed are transformed from the calibrated pixel numbers.
† The bonding of the wall with the substrate surface is not continuous.

spaced heights from the substrate surface. W_{min} means the minimum width of the wall that normally corresponds to the base of the wall. A geometrical variation coefficient η is introduced to express the width variation of each wall sample that is calculated from the following formula:

$$\eta = \left| \frac{W_a - W_{min}}{W_a} \right| \times 100\% \quad (6)$$

The geometrical change of the walls as a function of laser power is shown in Fig. 14. When no heat input control is applied, a preheating procedure contributes to the improvement of the geometrical accuracy of the wall, especially when the laser power is less than 500 W. With an increase in laser power, the influence of preheating becomes less important because a higher laser power can compensate for the heat loss for the different thermal conditions.

It can also be observed that, under all laser power levels, the geometrical variation in the cross-sections of the built walls with heat input control is much lower than those without control. When the laser power is below 400 W, there is nearly no width variation along the wall height if a control function is applied. Even at

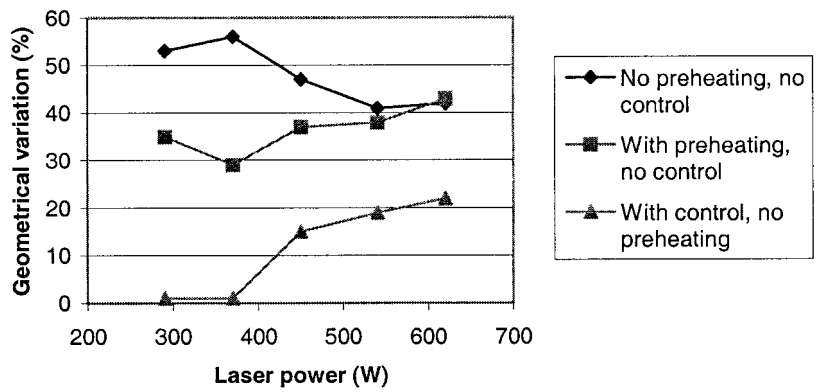

Fig. 14 Comparison of geometrical variation of laser cladding results

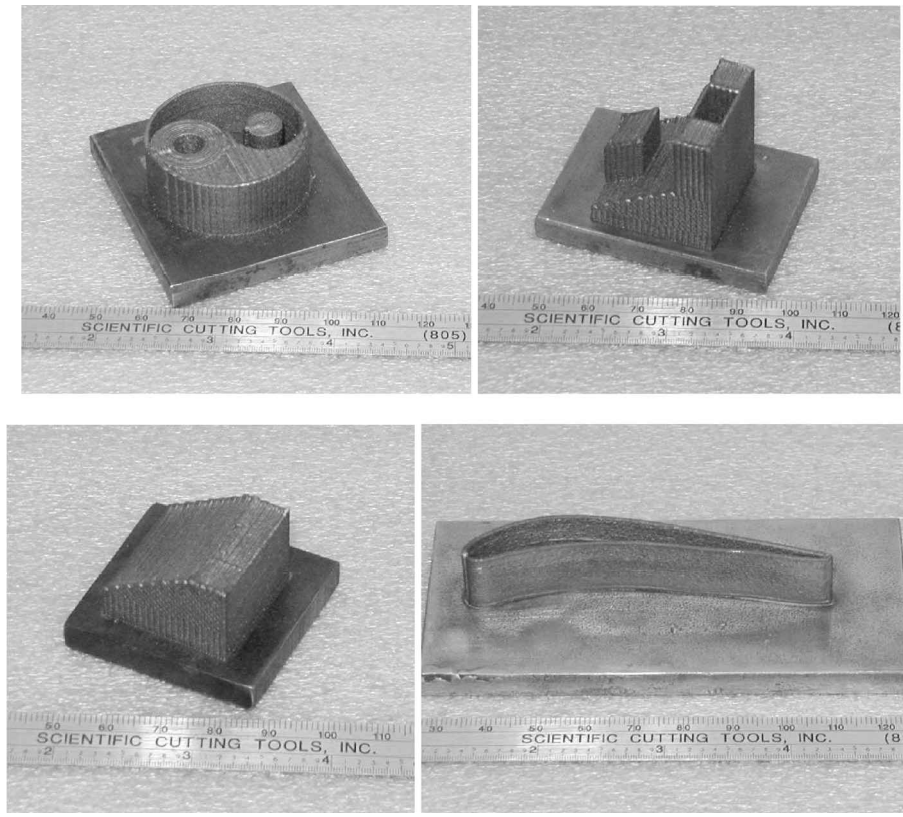

Fig. 15 Sample parts built by a closed-loop-controlled LBAM process

higher laser power levels, the geometrical accuracy gradually decreases but is still much higher than without the control function. More complex three-dimensional parts are built by closed-loop controlled LBAM process (Fig. 15). The parts show sufficient geometrical accuracies and fine surface qualities.

5 CONCLUSIONS

An opto-electronic sensor is developed that is capable of sensing the powder delivery rate in real time at a high sampling frequency. The sensing signal has a good linearity with the averaged powder delivery rate. The successfully developed powder delivery sensor is a base for further study on powder delivery control that ultimately will lead towards a precise, functionally gradient material delivery. Infrared image sensing is an efficient sensing method to improve the performance of LBAM. The coaxial installation of the camera ensures that clear infrared images of the molten pool and its surrounding thermal area can be acquired easily with a short nozzle–substrate distance and different scanning directions. The infrared image can eliminate the image noise caused by the metal powder and is easy to process in real time. The image reflects the temperature information that is a significant parameter affecting the cladding result. The closed-loop-controlled three-dimensional laser cladding based on infrared image sensing can overcome the effect of the thermal variation and thus achieve a consistent processing quality.

ACKNOWLEDGEMENTS

This work was financially supported by Texas Higher Education Coordinating Board (Grant 003613-0022-1999), the National Science Foundation (Grants DM1-9732848 and DM1-9809198) and the US Department of Education (Grant P200A80806-98).

REFERENCES

1 **Spencer, J. D., Dickens, P. M.** and **Wykes, C. M.** Rapid prototyping of metal parts by three-dimensional welding. *Proc. Instn Mech. Engrs, Part B, Journal of Engineering Manufacture*, 1998, **212**(B3), 175–182.

2 **Ribeiro, F., Norrish, J.** and **McMaster, R. S.** Practical case of rapid prototyping using gas metal arc welding. In Proceedings of the Conference on *Computer Technology in Welding*, Paris, France, 1994, paper 55.

3 **Rangel, R. H.** and **Bian, X.** Metal-droplet deformation and solidification model with substrate remelting. In Proceedings of the 1996 ASME International Mechanical Engineering Congress and Exposition, Atlanta, Georgia, 1996, Vol. 336, pp. 265–273 (American Society of Mechanical Engineers, New York).

4 **Das, S., Fuesting, T. P., Danyo, G., Brown, L. E., Beaman, J. J., Bourell, D. L.** and **Sargent, K.** Direct laser fabrication of gas turbine engine component-microstructure and properties. In *Solid Freeform Fabrication Proceedings* (Eds H. L. Marcus, J. J. Beaman, D. L. Bourell, J. W. Barlow and R. H. Crawford), Austin, Texas, 1998, pp. 1–18.

5 **Griffith, M. L., Keicher, D. M., Atwood, C. L., Romero, J. A., Smugeresky, J. E., Harwell, L. D.** and **Greene, D. L.** Free form fabrication of metallic components using laser engineered net shaping (LENS). In *Solid Freeform Fabrication Proceedings* (Eds D. L. Bourell, J. J. Beaman, H. L. Marcus, R. H. Crawford and J. W. Barlow), Austin, Texas, 1996, pp. 125–131.

6 **Link, G. R., Fessler, J., Nickel, A.** and **Prinz, F.** Rapid tooling die case inserts using shape deposition manufacturing. *Mater. Mfg Processes*, 1998, **13**(2), 263–274.

7 **Milewski, J. O., Lewis, G. K., Thoma, D. J., Keel, G. I., Nemec, R. B.** and **Reinert, R. A.** Directed light fabrication of a solid metal hemisphere using 5-axis powder deposition. *J. Mater. Processing Technol.*, 1998, **75**(1–3), 165–172.

8 **Yevko, V., Park, C. B., Zak, G., Coyle, T. W.** and **Benhabib, B.** Cladding formation in laser-beam fusion of metal powder. *Rapid Prototyping J.*, 1998, **4**(4), 168–184.

9 **Hu, D., Mei, H.** and **Kovacevic, R.** Closed loop control of 3D laser cladding based on infrared sensing. In *Solid Freeform Fabrication Proceedings* (Eds D. L. Bourell, J. J. Beaman, R. H. Crawford, H. L. Marcus, K. L. Wood and J. W. Barlow), Austin, Texas, 2001, pp. 129–137.

10 **Kmecko, I., Hu, D.** and **Kovacevic, R.** Controlling heat input, spatter and weld penetration in GMA welding for solid freeform fabrication. In *Solid Freeform Fabrication Proceedings* (Eds D. L. Bourell, J. J. Beaman, R. H. Crawford, H. L. Marcus and J. W. Barlow), Austin, Texas, 1999, pp. 735–742.

11 **Song, Y. A., Park, S., Jee, H., Choi, D.** and **Shin, B.** 3D welding and milling—a direct approach for fabrication of injection molds. In *Solid Freeform Fabrication Proceedings* (Eds D. L. Bourell, J. J. Beaman, R. H. Crawford, H. L. Marcus and J. W. Barlow), Austin, Texas, 1999, pp. 793–800.

12 **Verret, P.-A., Engel, Th.** and **Fontaine, J.** Laser cladding: the relevant parameters for process control. *Proc. Soc. Photo-opt. Instrumn Engrs*, 1998, **2207**, 452–462.

13 **Li, L.** and **Steen, W. M.** Sensing, modeling and closed loop control of powder feeder for laser surface modification. In Proceedings of the International Congress on *Applications of Lasers and Electro-Optics* (*ICALEO 1993*), 1993, pp. 965–974.

14 **Grunenwald, B., Nowotny, St., Henning, W., Dausinger, F.** and **Hugel, H.** New technology developments in laser cladding. In Proceedings of the International Congress on *Applications of Lasers and Electro-Optics* (*ICALEO 1993*), 1993, pp. 934–944.

15 **Jeng, J.-Y., Quayle, B., Modern, P. J.** and **Steen, W. M.** Computer control of laser multi-powder feeder cladding system for optimal alloy scan of corrosion and wear resistance. In Proceedings of the International Conference on *Laser Advanced Material Processing—Science and Application* (*LAMP '92*), 1992, pp. 819–824.

16 **Meriaudeau, F., Truchetet, F., Dumont, C., Renier, E.** and **Bolland, P.** Acquisition and image processing system able to optimize laser cladding process. In Proceedings of the 3rd International Conference on *Signal Processing* (*ICSP '96*), 1996, pp. 1628–1631.

17 **Romer, G. W., Hoeksma, M.** and **Meijer, J.** Industrial imaging controls laser surface treatment. *Photonics Spectra*, 1997, **31**(11), 104–109.

18 **Hu, D., Labudovic, M.** and **Kovacevic, R.** On line sensing of laser surface modification process by computer vision. In Proceedings of AWS 9th International Conference on *Computer Technology in Welding*, 1999, pp. 417–424.

19 **Hofmeister, W. H., MacCallum, D. O.** and **Knorovsky, G. A.** Video monitoring and control of the LENS process. In Proceedings of AWS 9th International Conference on *Computer Technology in Welding*, 1998, pp. 187–196.

20 **Mazumder, J., Dutta, D., Kikuchi, N.** and **Ghosh, A.** Closed loop direct metal deposition: art to part. *Optics Laser Engng*, 2000, **34**, 397–414.

